SAPIENZA
UNIVERSITÀ DI ROMA

MASTER'S DEGREE IN CONTROL ENGINEERING

Trajectory tracking and balancing for triple pendulum on a cart

UNDERACTUATED ROBOTS

Professor:
Leonardo Lanari

Students:
Carlo Rugiero
Diana Ioana Bubenek Turconi
Emanuele Coletta
Gianluca Sperduto

Academic Year 2025/2026

Contents

1 Introduction **2**
1.1 Triple pendulum on a cart: dynamic model 2
1.2 Overview of control approaches 5

2 Periodic orbit stabilization via BVP-LQR **6**
2.1 Feedforward control design via BVP 7
2.2 Feedback control design via LQR 9
2.3 Simulations 10

3 Trajectory tracking and balancing via Cascaded-EIC **16**
3.1 Cascaded-EIC 18
3.2 Control design 19
3.3 Simulations 22

Bibliography **26**

Chapter 1

Introduction

Underactuated systems are systems in which the number of control inputs is strictly less then the number of variables to control, i.e. the degrees of freedom. Those classes of systems are particularly challenging to treat from a control point of view, as the capability to actuate independently each subsystem is strongly limited, and control design is forced to take into account the natural internal dynamics of the system and the interconnection between the variables. Several notable examples of underactuated systems come from the robotics field: humanoids, manipulators affected by faults or educational robot as the Pendubot or Acrobot are some of them.

1.1 Triple pendulum on a cart: dynamic model

This project is focused on the control of a triple passive pendulum mounted on a actuated cart, or equivalently a PRRR planar robot. This robot, whose schematic is depicted in Figure 1.1, is described in configuration space by the 4-dimensional configuration vector $q = [x_c,\ \vartheta_1,\ \vartheta_2,\ \vartheta_3]^T$, whose components represent, respectively, the cart position and the three joint angles. By convention, zero configuration of the robot corresponds to the upward vertical position, which is an open loop unstable equilibrium for the pendulum. Furthermore, the joint angles represent the absolute orientation of the corresponding joint with respect to the vertical axis: this choice of parameter does not stick to the standard Denavit-Hartenberg convention.

The dynamics model of this robot can be obtained using a standard Euler-Lagrange approach [1]. To this aim, the Lagrangian function $\mathcal{L} = \mathcal{T} - \mathcal{U}$, where $\mathcal{T}$ is the total kinetic energy and $\mathcal{U}$ the total potential energy, is built, together with the Rayleigh function $\mathcal{R}$, which accounts for dissipative forces. Then, the dynamics model, expressed in the variables q and inputs τ, is obtained as

$$\frac{d}{dt}\left(\frac{\partial \mathcal{L}}{\partial \dot{q}_i}\right) - \frac{\partial \mathcal{L}}{\partial q_i} + \frac{\partial \mathcal{R}}{\partial \dot{q}_i} = \tau_i, \quad i = 0, \dots, 3, \tag{1.1}$$

where the cart is indexed as $i = 0$ and the revolute joints by $i = 1, 2, 3$.

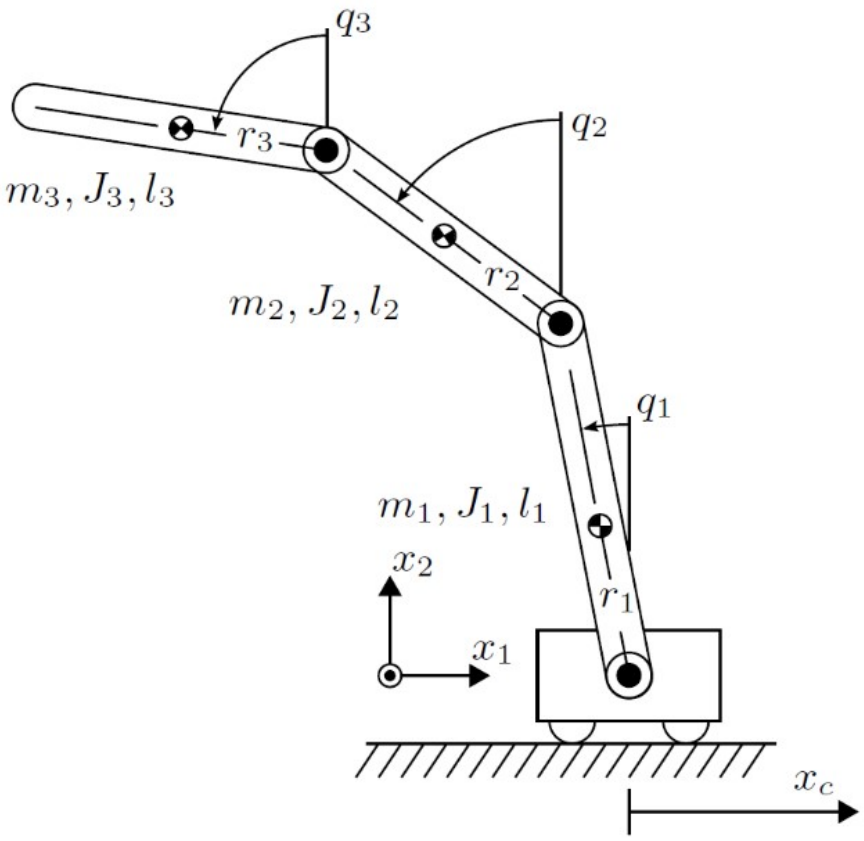

Figure 1.1: Schematic of a triple pendulum on a cart [3].

To obtain the analytical expressions of the energetic terms involved, let's denote by

- l_i the length of the i-th link,
- r_i the distance between the center of mass of the i-th link to the i-th joint,
- m_i the mass of the i-th link,
- J_i the inertia moment of the i-th link with respect to its center or mass (around an axis parallel to the axis of the i-th joint),
- d_i the viscous friction coefficient of the i-th joint,
- $G_0 = [0,\ -g_0]^T$ the gravity acceleration, with $g_0 = 9.81 \frac{m}{s^2}$.

The position of the center of mass of the four elements of the system can be expressed

as

$$
\begin{aligned}
p_{c0} &= \begin{bmatrix} x_c \\ 0 \end{bmatrix}, \\
p_{c1} &= \begin{bmatrix} x_c - r_1 \sin\vartheta_1 \\ r_1 \cos\vartheta_1 \end{bmatrix}, \\
p_{c2} &= \begin{bmatrix} x_c - l_1 \sin\vartheta_1 - r_2 \sin\vartheta_2 \\ l_1 \cos\vartheta_1 + r_2 \cos\vartheta_2 \end{bmatrix}, \\
p_{c3} &= \begin{bmatrix} x_c - l_1 \sin\vartheta_1 - l_2 \sin\vartheta_2 - r_3 \sin\vartheta_3 \\ l_1 \cos\vartheta_1 + l_2 \cos\vartheta_2 + r_3 \cos\vartheta_3 \end{bmatrix}.
\end{aligned} \tag{1.2}
$$

Then, the kinetic energy is

$$
\mathcal{T} = \frac{1}{2} m_0 \dot{x}_c^2 + \frac{1}{2} \sum_{i=1}^{3} \Big(m_i \dot{p}_{ci}^T \dot{p}_{ci} + J_i \omega_i^2 \Big), \tag{1.3}
$$

the potential energy is

$$
\mathcal{U} = G_0^T (m_1 p_{c1} + m_2 p_{c2} + m_3 p_{c3}) \tag{1.4}
$$

and the Rayleigh dissipation function is

$$
\mathcal{R} = \frac{1}{2} d_1 \dot{\vartheta}_1^2 + \frac{1}{2} d_2 (\dot{\vartheta}_2 - \dot{\vartheta}_1)^2 + \frac{1}{2} d_3 (\dot{\vartheta}_3 - \dot{\vartheta}_2)^2. \tag{1.5}
$$

As a result, a dynamic model of the form

$$
M(q)\ddot{q} + C(q,\dot{q})\dot{q} + D\dot{q} + g(q) = B\tau \tag{1.6}
$$

is obtained, where (for compactness, the standard notation $c_i = \cos\vartheta_i$, $s_i = \sin\vartheta_i$, $c_{ij} = \cos(\vartheta_i - \vartheta_j)$, $s_{ij} = \sin(\vartheta_i - \vartheta_j)$ is adopted):

- the positive definite inertia matrix $M(q)$ is

$$
M(q) = \begin{bmatrix}
m_0 + m_1 + m_2 + m_3 & -(r_1 m_1 + l_1 m_2 + l_1 m_3) c_1 & -(r_2 m_2 + l_2 m_3) c_2 & -r_3 m_3 c_3 \\
-(r_1 m_1 + l_1 m_2 + l_1 m_3) c_1 & J_1 + m_1 r_1^2 + (m_2 + m_3) l_1^2 & l_1 (r_2 m_2 + l_2 m_3) c_{12} & r_3 l_1 m_3 c_{13} \\
-(r_2 m_2 + l_2 m_3) c_2 & l_1 (r_2 m_2 + l_2 m_3) c_{12} & J_2 + m_2 r_2^2 + m_3 l_2^2 & r_3 l_2 m_3 c_{23} \\
-r_3 m_3 c_3 & r_3 l_1 m_3 c_{13} & r_3 l_2 m_3 c_{23} & J_3 + m_3 r_3^2
\end{bmatrix}, \tag{1.7}
$$

- the Coriolis matrix $C(q,\dot{q})$ is

$$
C(q,\dot{q}) = \begin{bmatrix}
0 & \dot{\vartheta}_1 (r_1 m_1 + l_1 m_2 + l_1 m_3) s_1 & \dot{\vartheta}_2 (r_2 m_2 + l_2 m_3) s_2 & \dot{\vartheta}_3 r_3 m_3 s_3 \\
0 & 0 & \dot{\vartheta}_2 l_1 (r_2 m_2 + l_2 m_3) s_{12} & \dot{\vartheta}_3 r_3 l_1 m_3 s_{13} \\
0 & -\dot{\vartheta}_1 l_1 (r_2 m_2 + l_2 m_3) s_{12} & 0 & \dot{\vartheta}_3 r_3 l_2 m_3 s_{23} \\
0 & -\dot{\vartheta}_1 r_3 l_1 m_3 s_{13} & -\dot{\vartheta}_2 r_3 l_2 m_3 s_{23} & 0
\end{bmatrix}, \tag{1.8}
$$

- the damping matrix D is

$$D = \begin{bmatrix} d_0 & 0 & 0 & 0 \\ 0 & d_1 + d_2 & -d_2 & 0 \\ 0 & -d_2 & d_2 + d_3 & -d_3 \\ 0 & 0 & -d_3 & d_3 \end{bmatrix}, \tag{1.9}$$

- the gravity vector $g(q)$ is

$$g(q) = \begin{bmatrix} 0 \\ -g_0(r_1 m_1 + l_1 m_2 + l_1 m_3)s_1 \\ -g_0(r_2 m_2 + l_2 m_3)s_2 \\ -g_0 r_3 m_3 s_3 \end{bmatrix} \tag{1.10}$$

- the input selection vector B is

$$B = \begin{bmatrix} 1 \\ 0 \\ 0 \\ 0 \end{bmatrix}. \tag{1.11}$$

1.2 Overview of control approaches

Two different control strategies are considered in this project to address the problem of generating and stabilizing non-trivial motions of the triple pendulum on a cart.

The first approach, proposed by Jahn, Watermann and Reger [3], aims at stabilizing the robot around a periodic orbit designed for the links of the pendulum. Control design follows a two-degrees-of-freedom structure. First, a nominal periodic orbit is generated offline by solving an inversion-based feedforward design problem, formulated as a two-point boundary value problem (BVP) for the internal dynamics of the system. The resulting trajectory is then locally stabilized by a time-varying Linear Quadratic Regulator (TV-LQR), designed along the nominal motion which results in a periodic solution of the associated differential Riccati equation. This approach is fully implemented and validated in simulation.

The second approach, introduced by Han and Yi [2], is based on a Cascaded External and Internal Convertible (CEIC) form and aims at tracking a reference trajectory for the cart while balancing the pendulum in the upward equilibrium. Cascaded-EIC extends the classical EIC framework to highly underactuated robots, where the number of unactuated coordinates is greater than the number of actuated ones, thus precisely the case of the triple pendulum on a cart. The control is built through a cascade of feedback linearizing loops, each addressing one level of the underactuation hierarchy by considering each joint virtually actuated by the previous one. We discuss the theoretical foundations of the method and investigate its applicability to our system.

Chapter 2

Periodic orbit stabilization via BVP-LQR

The first approach considered in this project is the one proposed in [3], where the objective is to generate and stabilize a non trivial periodic orbit for the pendulum. This method follows a 2-DOF structure: first, a nominal periodic trajectory is generated by solving an inversion-based feedforward design problem, formulated as a two-poind boundary value (BVP) problem for the internal dynamics; then, a time-varying LQR controller is designed along the nominal motion to render it attractive.

As detailed in the first chapter, the triple passive pendulum on a cart is a system described in configuration space by the $n_q = 4$ generalized coordinates of the configuration vector

$$q = \begin{bmatrix} x_c & \vartheta_1 & \vartheta_2 & \vartheta_3 \end{bmatrix}^T, \tag{2.1}$$

where x_c is the cart position and $\eta = [\vartheta_1, \vartheta_2, \vartheta_3]$ are the pendulum angles measured with respect to the vertical. The full nonlinear dynamics is written as

$$M(q)\ddot{q} + C(q, \dot{q})\dot{q} + g(q) + D\dot{q} = S\tau, \tag{2.2}$$

where τ is the force applied to the cart and

$$S = \begin{bmatrix} 1 & 0 & 0 & 0 \end{bmatrix}^T. \tag{2.3}$$

The system therefore possess $m = 1$ degrees of actuation and $n_q - m = 3$ degrees of unactuation. Moreover, considering x_c as output, the system has relative degree $r = 2$, and the internal zero dynamics has dimension $n - r = 6$, corresponding to the states associated to the pendulum dynamics $(\eta, \dot{\eta})$.

Due to the structure of the system, it is always possible to transform the dynamics of the cart in a double integrator by feedback linearization of the first row of 2.2, leading to

$$\begin{cases} \ddot{x}_c = u \\ M(\eta)\ddot{\eta} + C(\eta, \dot{\eta})\dot{\eta} + g(\eta) + D\dot{\eta} + b(\eta)u = 0 \end{cases} \tag{2.4}$$

where:

- $M(\eta) \in \mathbb{R}^{3\times3}$ is the reduced inertia matrix,
- $C(\eta, \dot{\eta}) \in \mathbb{R}^{3\times3}$ is the reduced Coriolis matrix,
- $g(\eta) \in \mathbb{R}^3$ is the reduced gravity vector,
- $D \in \mathbb{R}^{3\times3}$ is the reduced viscous friction matrix,
- $b(\eta) \in \mathbb{R}^3$ captures the coupling between cart acceleration and joint accelerations.

In this way, the dynamics of the cart is fully decoupled from the dynamics of the joints. Since neither the cart position nor its velocity appear in the above terms, it is possible to consider the cart acceleration as a virtual input for the pendulum, whose dynamics is shaped through the coupling term $b(\eta)$.

In summary, the original 4-dimensional system has been transformed into an input-output normal form, where the observable dynamics is just the scalar double integrator $\ddot{x}_c = u$ and the internal dynamics is the 3-dimensional subsystem

$$\ddot{\eta} = \beta_f(\eta, \dot{\eta}) + \beta_g(\eta)u, \tag{2.5}$$

where

$$\beta_f(\eta, \dot{\eta}) = -M^{-1}(\eta)\Big(C(\eta, \dot{\eta})\dot{\eta} + g(\eta) + D\dot{\eta}\Big) \in \mathbb{R}^3 \tag{2.6}$$

is the drift vector and

$$\beta_g(\eta) = -M^{-1}b(\eta) \in \mathbb{R}^3 \tag{2.7}$$

is the input vector.

The control design for this affine nonlinear system Σ follows the typical two degrees of freedom depicted in Figure 2.1, where the feedforward term Σ_{FF} is designed to generate the reference command to make Σ behave as Σ_{TG} in ideal settings and the feedback term Σ_{FB} is responsible for tracking it based on the real measurements from the system. The scheme also shows the observer $\tilde{\Sigma}$ needed to reconstruct the internal state variables from the measured output; this aspect is however not taken into account in this work.

2.1 Feedforward control design via BVP

The feedforward controller aims at designing a periodic orbit for the pendulum links and it is obtained by solving an appropriately defined two-points boundary value problem (BVP). While in a standard Cauchy problem the boundary condition is specified only at one endpoint, A two-points boundary value problem is the problem of obtaining a function defined over the interval $[0, T]$ that is solution of a given differential equation and satisfies boundary conditions specified both for $t = 0$ and $t = T$. The additional constraints make solving a BVP harder than a standard Cauchy problem, hence numerical methods are employed. In this work, the `bvp5c` function in MATLAB is used.

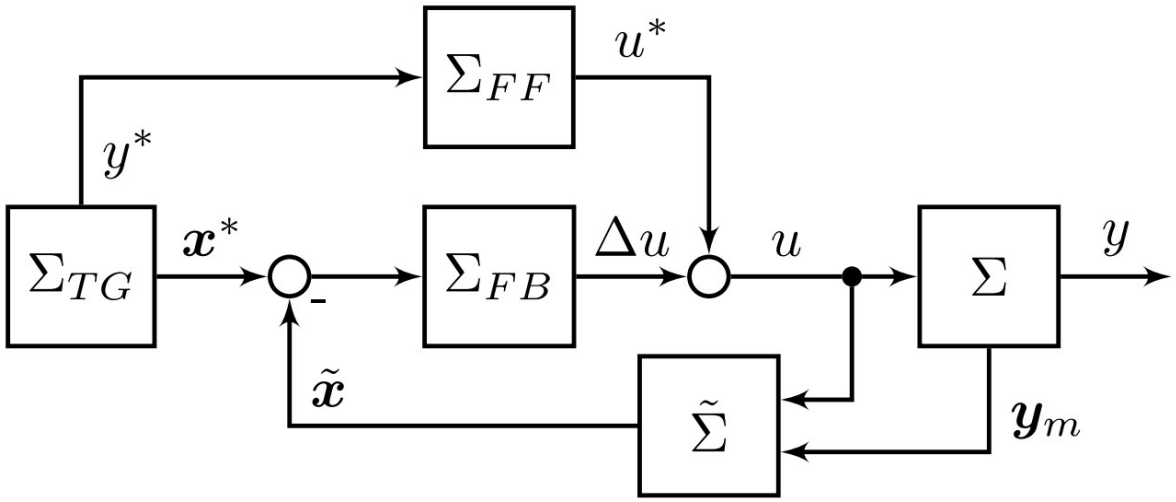

Figure 2.1: 2-DoF control scheme.

The desired output motion is generated by parametrizing the cart position $x_c(t)$ as a finite sum of sinusoidal basis functions depending on a parameter vector $p \in \mathbb{R}^6$:

$$x_c(t) = \Upsilon(t,p) = \sum_{i=1}^{2} a_i \sin\Big(\frac{i\pi t}{T}\Big) + \sum_{i=1}^{6} p_i \sin\Big(\frac{(2+i)\pi t}{T}\Big). \tag{2.8}$$

The sin functions are chosen as interpolating polynomials to enforce periodicity of motion. To obtain the parameters p_i, the associated BVP is solved using `bvp5c`, where the differential equation to satisfy is the dynamic model of the robot

$$\ddot{\eta} = \beta_f(\eta, \dot{\eta}) + \beta_g(\eta)\ddot{\Upsilon}(t,p) \tag{2.9}$$

with the boundary conditions enforced by the desired orbit.

For example, with

$$\begin{cases} \eta_i(0) = 0 \\ \dot{\eta}_i(0) = \dot{\eta}_{i,0} \end{cases} \quad \text{and} \quad \begin{cases} \eta_i(T) \in \{0, 2\pi\} \\ \dot{\eta}_i(T) = \dot{\eta}_{i,0} \end{cases} \qquad i = 1,2,3. \tag{2.10}$$

the orbit starts from the upward position with a predetermined speed $(\dot{x}_{c,0}, \dot{\eta}_{i,0})$; furthermore, joint i undergoes a full rotation if $\eta_i(T) = 2\pi$ while it is simply balanced around its vertical equilibrium if $\eta_i(T) = 0$. Choosing a sine series of period T as solution to the BVP ensures that the cart returns to $x_c = 0$ after one period, without explicitly adding another boundary condition.

Once the optimal parameters $p^\star$ are obtained, the cart acceleration

$$u^\star(t) = \ddot{x}_c(t, p^\star) \tag{2.11}$$

is injected into the complete model and integrated forward in time to verify that the boundary conditions are satisfied and the desired motion is achieved.

2.2 Feedback control design via LQR

The feedforward control alone does not guarantee robustness with respect to disturbances or model uncertainties. For this reason, a local feedback controller based on a time-varying Linear Quadratic Regulator (TV-LQR) is designed along the nominal trajectory in order to make the reference trajectory attractive.

In its state space formulation, the robot dynamics can be written in compact form as

$$\dot{x} = F(x, u) = f(x) + g(x)u, \tag{2.12}$$

i.e. as a nonlinear affine dynamical system, where the 8-dimensional state

$$x = \begin{bmatrix} x_c & \eta & \dot{x}_c & \dot{\eta} \end{bmatrix}^T \tag{2.13}$$

includes both joint positions and their velocities. Let $x^\star(t)$ and $u^\star(t)$ denote the nominal state and input obtained from the BVP.

Linearizing around the nominal trajectory yields the time-varying system

$$\delta\dot{x} = A(t)\delta x + B(t)\delta u, \tag{2.14}$$

where

$$A(t) = \left.\frac{\partial F(x,u)}{\partial x}\right|_{\left(x^\star(t),u^\star(t)\right)} \in \mathbb{R}^{8\times 8} \tag{2.15}$$

is the linearized dynamic matrix and

$$B(t) = \left.\frac{\partial F(x,u)}{\partial u}\right|_{\left(x^\star(t),u^\star(t)\right)} = g\big(x^\star(t)\big) \in \mathbb{R}^8 \tag{2.16}$$

is the linearized input vector. This linear model describes the evolution of small deviations $\delta x = x - x^\star$ and $\delta u = u - u^\star$ along the orbit.

The feedback gain is computed by minimizing the quadratic performance index

$$J(\delta x, \delta u) = \int_0^T \Big(\delta x^T Q \delta x + \delta u^T R \delta u\Big)\, dt, \tag{2.17}$$

where $Q \succeq 0$ penalizes state deviations and $R \succ 0$ penalizes control effort.

The optimal time-varying gain is obtained from the solution of the differential Riccati equation

$$-\dot{X} = XA + A^T X - XBR^{-1}B^T X + Q, \tag{2.18}$$

integrated backward in time with terminal condition

$$X(T) = X_T, \tag{2.19}$$

where X_T is computed from the continuous algebraic Riccati equation evaluated at the final point of the trajectory for the periodic orbit phase. For the transition maneuvers

(swing-up, entry, defuse, swing-down), the terminal condition is instead set to $X_T = 0$, which is a standard choice when no specific terminal cost is imposed. A solution that enforces a *Positive Definite T-Periodic Matrix Solution* can be obtained by solving the Riccati equation for multiple periods, with final condition $X(T) = Q_T = 0_{8\times 8}$ (Theorem 1 of [3]).

Once the positive definite T-periodic matrix $X(t)$ has been found, the feedback gain is then

$$K(t) = -R^{-1}B^T(t)X(t) \tag{2.20}$$

and the resulting control law making the reference orbit locally stable and attractive is

$$u(t) = u^\star(t) - K(t)\Big(x(t) - x^\star(t)\Big). \tag{2.21}$$

In our implementation, to obtain numerical convergence, we first integrate the Riccati equation over 10 cycles (for a time $\bar{T} = 10T$) to drive the gain toward a periodic solution, and then reintegrate over 2 cycles starting from the converged terminal condition to obtain the final periodic gain. This multi-cycle procedure is not applied to the transition maneuvers, for which a single backward pass over the maneuver duration is sufficient. Moreover, the gain $K(t)$ is interpolated over time to obtain a continuous feedback function. Angular errors are evaluated using a circular error definition in order to correctly handle 2π wrapping of the joint coordinates.

2.3 Simulations

In this section we show some simulations carried out with the approach explained above. Apart from a periodic trajectory of the links, we leverage the method for swing-up, swing-down, entry, and defuse manoeuvrers as well. A complete simulation always starts with the robot being in his vertical downwards equilibrium, then a sequence of manoeuvrers are executed (including a periodic orbit for the third joint rotation), and finally the robot is returned to the downwards equilibrium. In summary, the complete simulation is composed by the following phases.

- Swing-up: to move the robot from the downward equilibrium to the upward equilibrium (Figure 2.5);
- Entry: to put the robot in motion, reaching the desired initial conditions for the periodic (Figure 2.6);
- Periodic orbit: with one full rotation of the third joint alone each period (Figures 2.2, 2.3, 2.4);
- Defuse: opposite of the entry manoeuvrer, this is used to exit the periodic motion and stop the robot in its upward equilibrium (Figure 2.7);

- Swing-down: to move the robot from the upward equilibrium back to the downward equilibrium in a controlled manner (Figure 2.8).

Each phase is generated via BVP and stabilized with its corresponding TV-LQR controller of the form

$$u(t) = u^{\star}(t) - K(t)\Big(x(t) - x^{\star}(t)\Big). \tag{2.22}$$

Each period of the cyclic motion starts and ends with $\dot{\eta}_0 = \dot{\eta}_T = 1.89$ rad/s and lasts for $T = 1.096s$. With initial guess for the BVP parameters of $p_0 = \begin{bmatrix} 0.01 & 0.01 & 0.01 & 0.01 & 0.01 & 0.01 \end{bmatrix}^T$, the obtained parameters are $p = \begin{bmatrix} -0.0138 & 0.0912 & 0.0258 & -0.0104 & -0.0127 & -0.0165 \end{bmatrix}^T$. The dynamic parameters are the same listed in [3].

A full rotation of the third link is enforced by using $\eta_0 = \mathbf{0}$ as initial condition and $\eta_T = \begin{bmatrix} 0 & 0 & 2\pi \end{bmatrix}$ as final condition for the poles angles.

Figure 2.2 shows the poles and cart trajectories used for the feedforward trajectories. The acceleration of the cart is used the control input after partial feedback linearization. LQR gains are tuned empirically. Better stability was observed when tuning gains on two periods instead of only one.

As mentioned in [3], the BVP approach can be used to design non-periodic trajectories as well, and feedback implemented with appropriate final conditions for the LQR Riccati equation. Swing-up and Swing-down manoeuvrers are shown in Figures 2.5 and 2.8, both starting and ending with null velocities and used to switch between the two equilibrium points of interest. Entry and defuse manoeuvres are instead used to enter or exit the periodic orbit, and also impose non-null desired velocities, as shown in Figures 2.6 and 2.7.

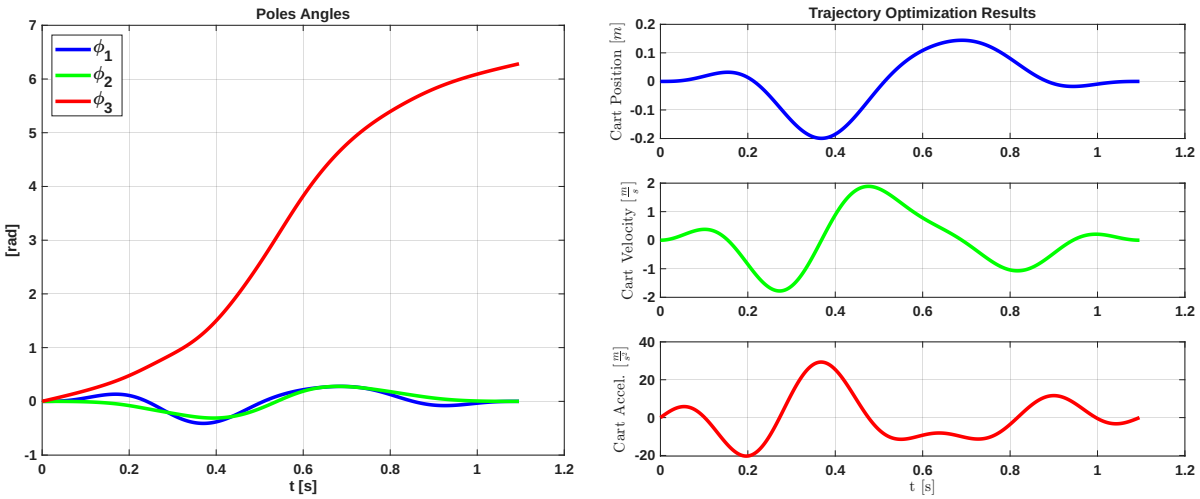

(a) Poles trajectory obtained from BVP solution for Cyclic orbit.

(b) Cart trajectory obtained from BVP solution for Cyclic orbit.

Figure 2.2: Trajectory obtained from BVP solution for Cyclic orbit.

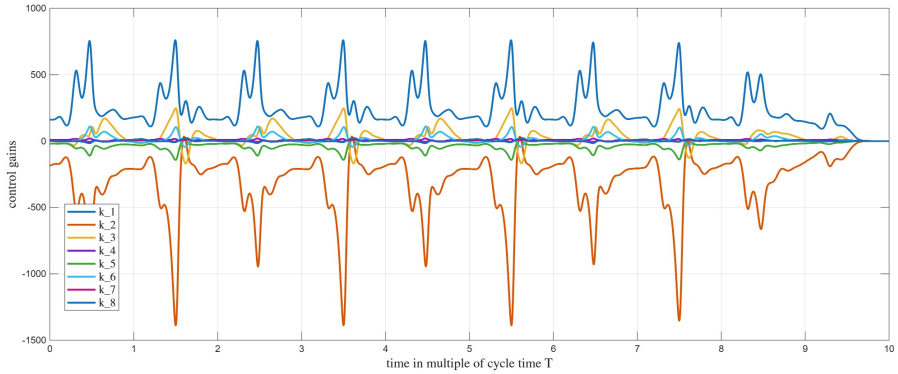

(a) Riccati gains obtained.

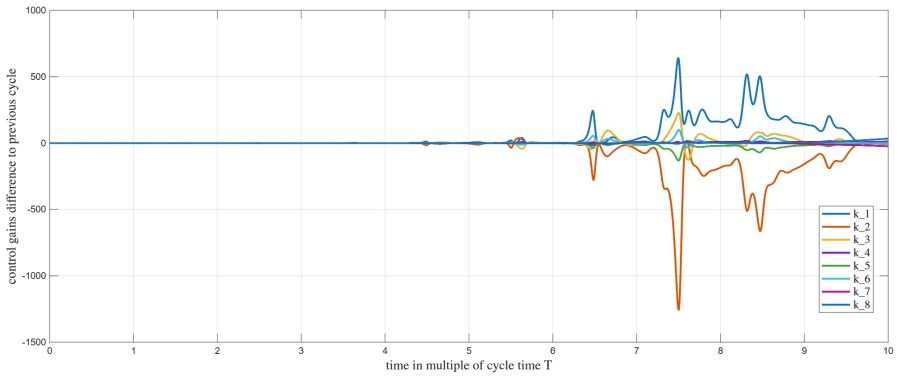

(b) Riccati Gains errors for 2 period cycles.

Figure 2.3: Periodicity of Riccati gains.

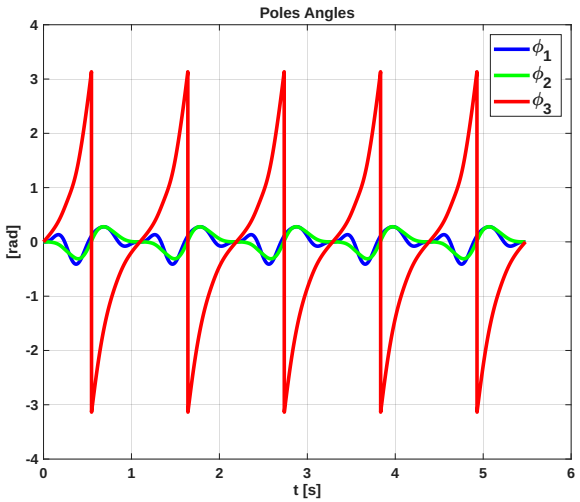

(a) Poles trajectory obtained from simulation of 5 cycles.

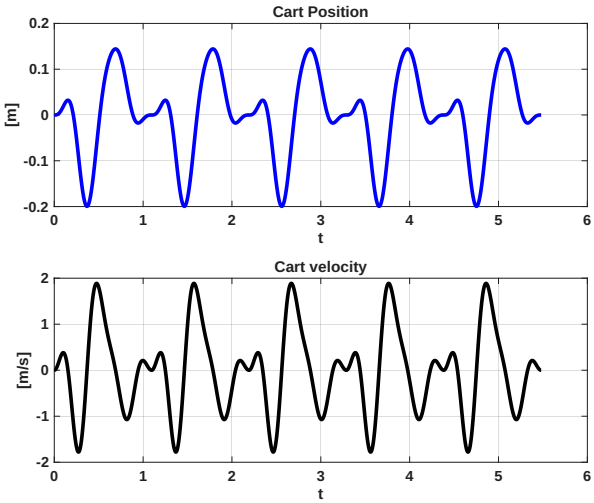

(b) Cart trajectory obtained from simulation of 5 cycles.

Figure 2.4: Simulation of 5 cycles periodic orbit with Feedback (LQR) and Feedforward (BVP ideal traj.).

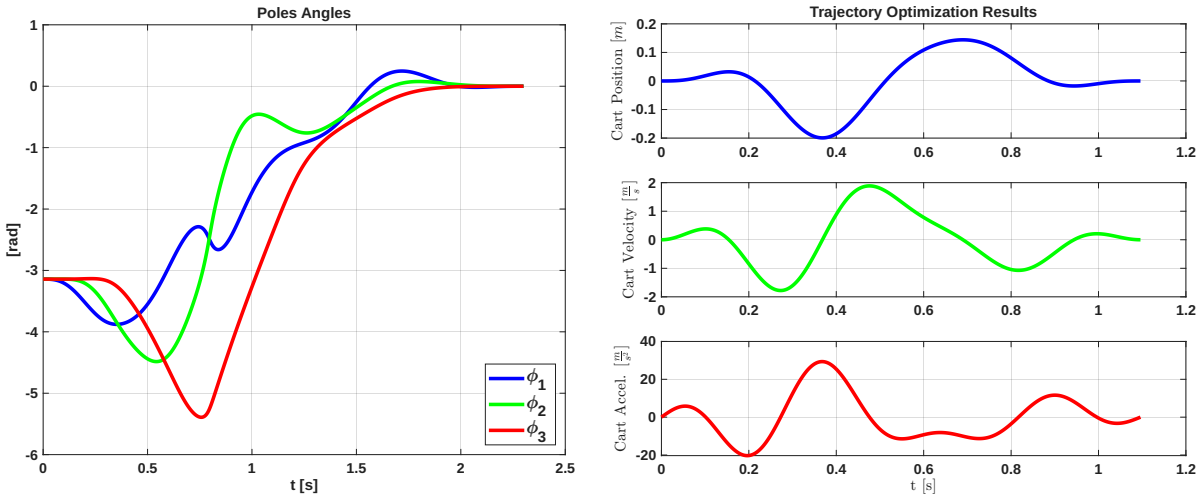

(a) Pendulum (b) Cart

Figure 2.5: Swing-up trajectory

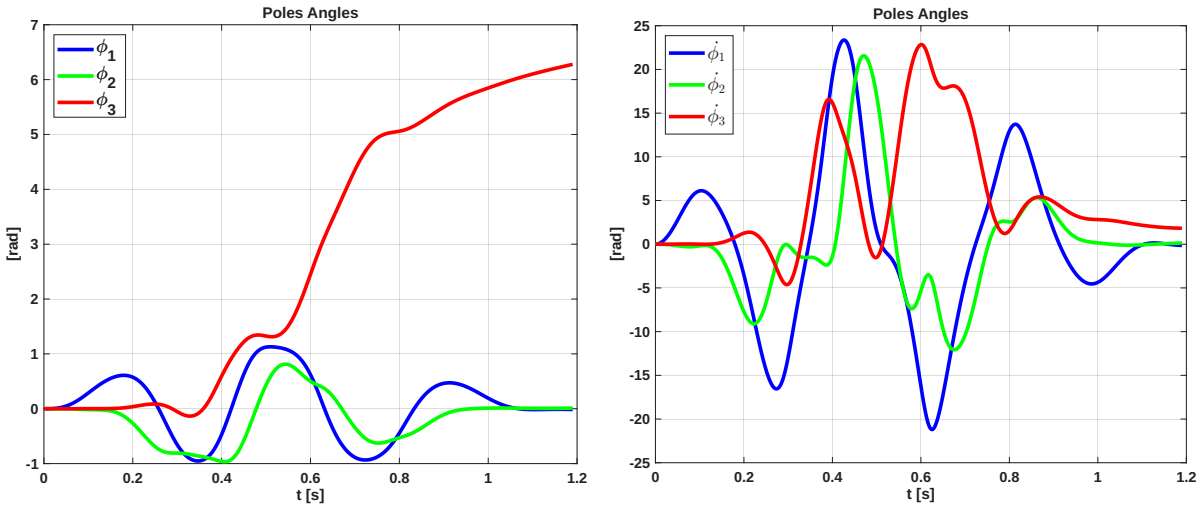

(a) Poles angles (b) Poles velocities

Figure 2.6: Entry manoeuvrer

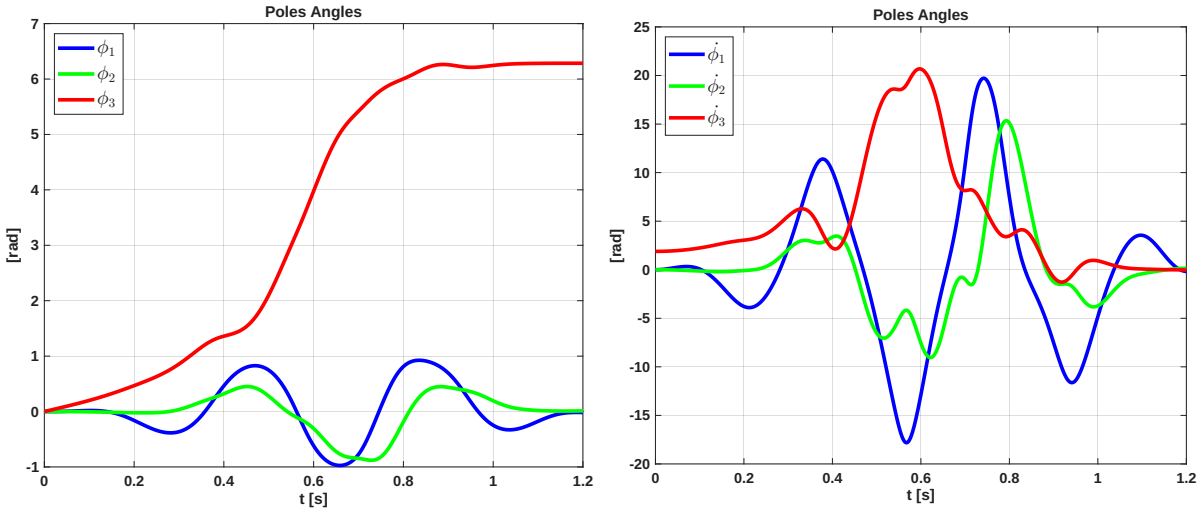

(a) Poles position

(b) Poles velocities

Figure 2.7: Defuse manoeuvrer

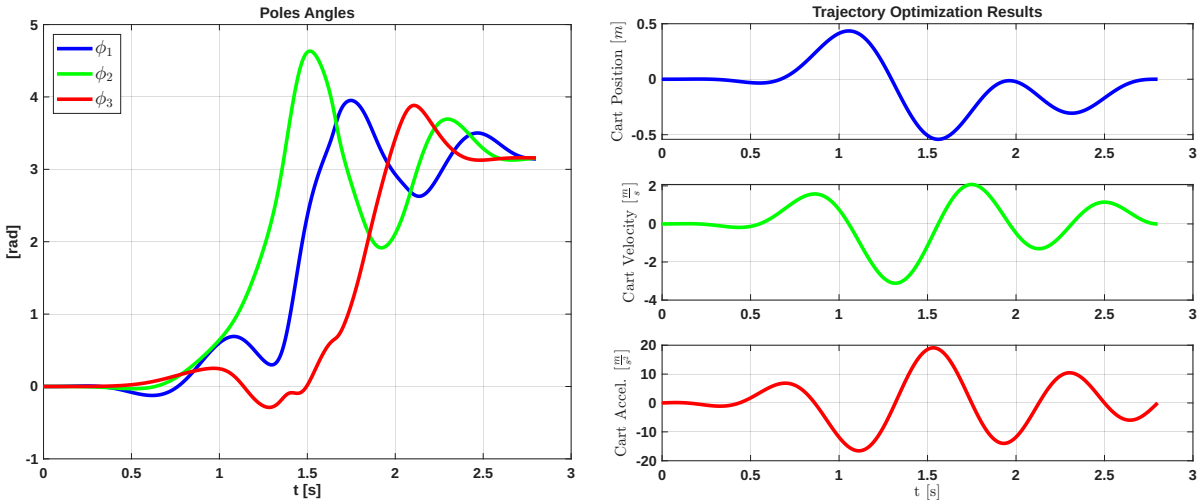

(a) Pendulum

(b) Cart

Figure 2.8: Swing-down trajectory

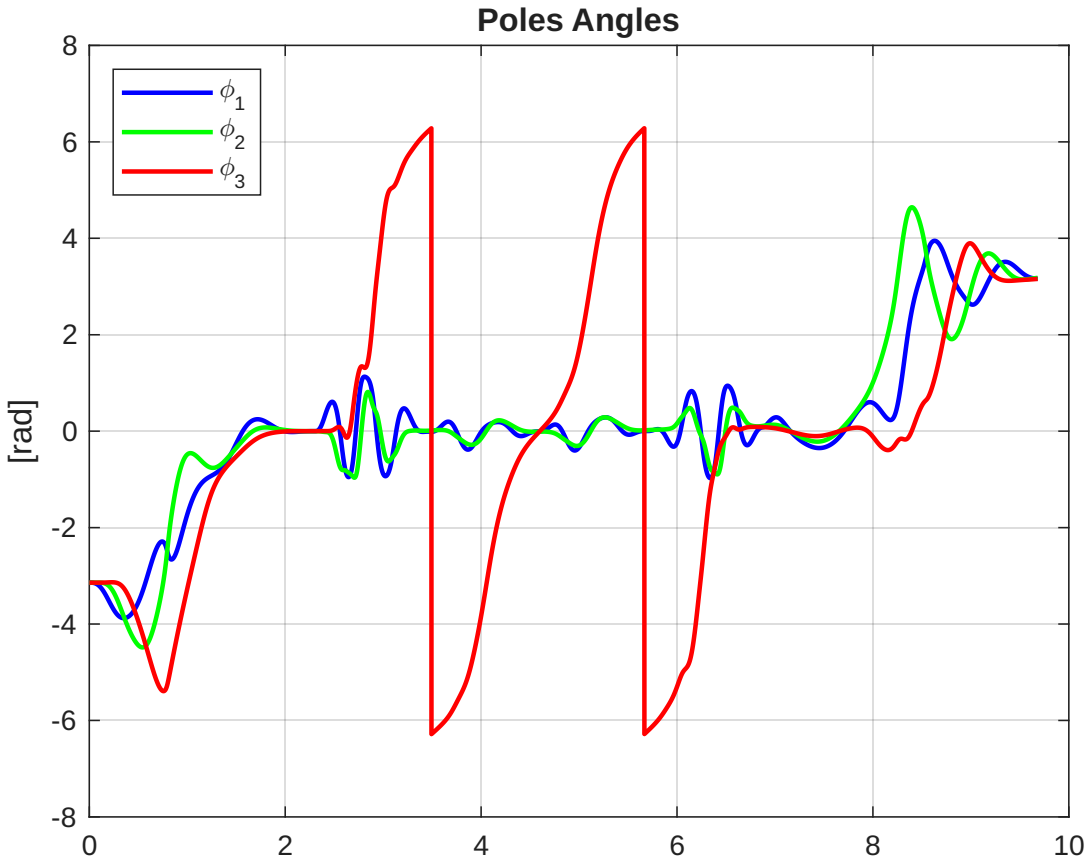

Figure 2.9: Complete simulation with all manoeuvrers

Chapter 3

Trajectory tracking and balancing via Cascaded-EIC

The second approach to trajectory tracking and balancing of an underactuated robot has been introduced in [2] and it is based on cascaded external and internal convertible form-based control (i.e., CEIC-based control). In the following, we shall denote $D(q) \coloneqq M(q), H(q) = C(q, \dot{q}) + G(q)$ to remain consistent with the notation used by the authors. Moreover, we shall ignore friction terms.

For the triple pendulum on a cart, the dynamics can be written as

$$\begin{bmatrix} D_{11} & D_{12} & D_{13} & D_{14} \\ D_{21} & D_{22} & D_{23} & D_{24} \\ D_{31} & D_{32} & D_{33} & D_{34} \\ D_{41} & D_{42} & D_{43} & D_{44} \end{bmatrix} \begin{bmatrix} \ddot{x}_c \\ \ddot{\vartheta}_1 \\ \ddot{\vartheta}_2 \\ \ddot{\vartheta}_3 \end{bmatrix} + \begin{bmatrix} H_1 \\ H_2 \\ H_3 \\ H_4 \end{bmatrix} = \begin{bmatrix} u \\ 0 \\ 0 \\ 0 \end{bmatrix}, \tag{3.1}$$

This model can be partitioned into the dynamics of the actuated variable q_a of dimension $n = 1$ and of the unactuated variables q_u of dimension $m = 3$, leading to

$$\begin{cases} D_{aa}\ddot{q}_a + D_{au}\ddot{q}_u + H_a = u \\ D_{ua}\ddot{q}_a + D_{uu}\ddot{q}_u + H_u = 0 \end{cases} \tag{3.2}$$

where

$$q_a = x_c, \qquad q_u = \begin{bmatrix} \vartheta_1 \\ \vartheta_2 \\ \vartheta_3 \end{bmatrix}, \tag{3.3}$$

$$D_{aa} = D_{11}, \qquad D_{au} = \begin{bmatrix} D_{12} & D_{13} & D_{14} \end{bmatrix}, \tag{3.4}$$

$$D_{ua} = \begin{bmatrix} D_{21} \\ D_{31} \\ D_{41} \end{bmatrix}, \quad D_{uu} = \begin{bmatrix} D_{22} & D_{23} & D_{24} \\ D_{32} & D_{33} & D_{34} \\ D_{42} & D_{43} & D_{44} \end{bmatrix}, \tag{3.5}$$

$$H_a = H_1, \qquad H_u = \begin{bmatrix} H_2 \\ H_3 \\ H_4 \end{bmatrix}. \tag{3.6}$$

In the classical EIC approach, which can be only used for slightly underactuated robots where $n \geq m$, the control goal is to track a reference trajectory q_a^d for the actuated variables while balancing the unactuated ones. The control design follows two steps.

In the first step, called external loop, a control u_a^{ext} is designed via feedback linearization of the actuated dynamics

$$u_a^{ext} = D_{aa} v_a^{ext} + D_{au} \ddot{q}_u + H_a. \tag{3.7}$$

This control imposes the dynamics $\ddot{q}_a = v_a^{ext}$ hence v_a^{ext} is designed to make the tracking error $e_a = q_a^d - q_a$ globally asymptotically stable as

$$v_a^{ext} = \ddot{q}_a^d + k_{d1} \dot{e}_a + k_{p1} e_a. \tag{3.8}$$

After that, the reference instantaneous equilibrium trajectory q_u^e for the unactuated variables is computed through the unactuated dynamics by imposing $\ddot{q}_a = v_a^{ext}$, $\dot{q}_u = 0$ and $\ddot{q}_u = 0$, leading to

$$D_{ua} v_a^{ext} + H_u|_{\dot{q}_u = 0} = 0. \tag{3.9}$$

This equation defines the set values for the unactuated variables that are instantaneously in equilibrium for the control v_a^{ext} acting on the system. This set is called Balance Equilibrium Manifold (BEM) and it is defined as

$$\mathcal{E} = \{q_u^e : \Gamma(q_u, v_a^{ext}) = 0, \dot{q}_u = 0, \ddot{q}_u = 0\}, \tag{3.10}$$

where

$$\Gamma(q_u, v_a^{ext}) = \tag{3.11}$$

Once this is settled, the second step, i.e. the internal loop, aims at designing a new value for v_a, namely v_a^{int}, to make the tracking error $e_u = q_u^e - q_u$ globally asymptotically stable. Employing again a feedback linearization approach,

$$v_a^{int} = -D_{ua}^{\#}(D_{uu} v_u^{int} + H_u), \tag{3.12}$$

where $D_{ua}^{\#}$ is the pseudoinverse of D_{ua}, imposes $\ddot{q}_u = v_u^{int}$, and

$$v_u^{int} = \ddot{q}_u^e + k_{d2} \dot{e}_u + k_{p2} e_u \tag{3.13}$$

solves the problem.

In conclusion, the full control law is

$$u_a^{int} = D_{aa} v_a^{int} + D_{au} \dot{q}_u + H_a = -D_{aa} D_{ua}^{\#}(D_{uu} v_u^{int} + H_u) + D_{au} \dot{q}_u + H_a. \tag{3.14}$$

This control makes q_u track q_u^e and, due to the way q_u^e was computed, makes also q_a track q_a^d. The limit of this approach is that it only works if there is no loss of information in the pseudoinverse $D_{ua}^{\#}$, otherwise it would not be possible to impose exactly the dynamics $\ddot{q}_a = v_a^{ext}$. In other words, this approach only works when $n \geq m$. For highly underactuated robots, instead, where $n < m$, the dynamics of q_u in closed loop with v_a^{ext} is still an underactuated system.

3.1 Cascaded-EIC

To solve this issue, in the cascaded EIC approach the design presented above is re-iterated for the underactuated subsystem until it leads to a fully actuated one. By isolating acceleration of actuated coordinates $\ddot{q}_a$ from the dynamics

$$\ddot{q}_a = (D_{aa})^{-1}(u - D_{au}\ddot{q}_u - H_u) \tag{3.15}$$

then plugging it into the unactuated system dynamics it is obtained

$$(D_{uu} - D_{ua}D_{aa}^{-1}D_{au})\ddot{q}_u + (H_u - D_{ua}D_{aa}^{-1}H_a) = -D_{ua}D_{aa}^{-1}u, \tag{3.16}$$

or, by defining

$$\begin{aligned} q^{(1)} &= q_u, \\ B^{(1)} &= -D_{ua}D_{aa}^{-1}, \\ D^{(1)} &= D_{uu} - D_{ua}D_{aa}^{-1}D_{au}, \\ H^{(1)} &= H_u - D_{ua}D_{aa}^{-1}H_a, \end{aligned} \tag{3.17}$$

one has

$$\mathcal{S}_1 : D^{(1)}\ddot{q}^{(1)} + H^{(1)} = B^{(1)}u. \tag{3.18}$$

For highly underactuated robots, this is still an underactuated dynamics, with m variables and n inputs, and the EIC approach can be applied again. In particular, the system is partitioned into

$$\begin{cases} D_{aa}^{(1)}\ddot{q}_a^{(1)} + D_{au}^{(1)}\ddot{q}_u^{(1)} + H_a^{(1)} = B_a^{(1)}u \\ D_{ua}^{(1)}\ddot{q}_a^{(1)} + D_{uu}^{(1)}\ddot{q}_u^{(1)} + H_u^{(1)} = B_u^{(1)}u \end{cases} \tag{3.19}$$

i.e. in a system very similar to the previous case, except for the presence of the input matrices $B_a^{(1)}$ and $B_u^{(1)}$, which in the original case were just the identity and zero matrices respectively. For the triple pendulum on a cart, $\dim(q^{(1)}) = 3$, $\dim(q_a^{(1)}) = 1$ and $\dim(q_u^{(1)}) = 2$. The underactuated part is still a highly underactuated one, hence another step is needed, leading to

$$\mathcal{S}_2 : D^{(2)}\ddot{q}^{(2)} + H^{(2)} = B^{(2)}u, \tag{3.20}$$

where

$$\begin{aligned} q^{(2)} &= q_u^{(1)}, \\ B^{(2)} &= B_u^{(1)} - D_{ua}^{(1)}(D_{aa}^{(1)})^{-1}B_a^{(1)}, \\ D^{(2)} &= D_{uu}^{(1)} - D_{ua}^{(1)}(D_{aa}^{(1)})^{-1}D_{au}^{(1)}, \\ H^{(2)} &= H_u^{(1)} - D_{ua}^{(1)}(D_{aa}^{(1)})^{-1}H_a^{(1)}. \end{aligned} \tag{3.21}$$

For the triple pendulum on a cart, $\dim(q^{(2)}) = 2$, hence the partition in the actuated and underactuated subsystems finally leads to a slightly underactuated system where $\dim(q_a^{(2)}) = 1$ and $\dim(q_u^{(2)}) = 1$.

Performing one last time the cyclic procedure bring the system in the form

$$\mathcal{S}_3 : D^{(3)}\ddot{q}^{(3)} + H^{(3)} = B^{(3)}u \tag{3.22}$$

where similarly to (3.21)

$$\begin{aligned} q^{(3)} &= q_u^{(2)}, \\ B^{(3)} &= B_u^{(2)} - D_{ua}^{(2)}(D_{aa}^{(2)})^{-1}B_a^{(2)}, \\ D^{(3)} &= D_{uu}^{(2)} - D_{ua}^{(2)}(D_{aa}^{(2)})^{-1}D_{au}^{(2)}, \\ H^{(3)} &= H_u^{(2)} - D_{ua}^{(2)}(D_{aa}^{(2)})^{-1}H_a^{(2)}. \end{aligned} \tag{3.23}$$

In this way, a fully actuated system is finally obtained.

To each sub-system (i) is associated a BEM equation for the underactuated part defined as

$$\mathcal{E}_i = \Big\{ q_u^{(i),e} : \Gamma_{i+1}(q_a^{(i+1)}, u) = 0, \dot{q}_a^{(i+1)} = \ddot{q}_a^{(i+1)} = 0 \Big\}, \tag{3.24}$$

where

$$\Gamma_{i+1} = D_{aa}^{(i+1)}\ddot{q}_a^{(i+1)} + D_{au}^{(i+1)} + H_a^{(i+1)} - B_a^{(i+1)}u. \tag{3.25}$$

Solving the BEM equation gives the reference instantaneous equilibrium $q_u^{(i),e}$

3.2 Control design

The first coordinate can be driven wherever desired just by imposing a feedback that partially linearizes the dynamics, as for the standard EIC , leading to

$$u_0^{ext} = (B_a^{(0)})^{-1}\Big(D_{aa}^{(0)}v_0^{ext} + D_{au}^{(0)}\ddot{q}_u^{(0)} + H_a^{(0)} \Big) \tag{3.26}$$

and

$$v_0^{ext} = \ddot{q}_a^{(0),d} + k_D(\dot{q}_a^{(0),d} - \dot{q}_a^{(0)}) + k_P(q_a^{(0),d} - q_a^{(0)}). \tag{3.27}$$

Balance of the underactuated system is achieved by exploting the BEM $\mathcal{E}_1 = \{q_u^{(1),e} = \begin{bmatrix} \vartheta_1 & \vartheta_2 & \vartheta_3 \end{bmatrix}^T\}$ obtained solving Γ_1. From the obtained solution, only the first n coordinates are used, that in our case is just $q_{u,1}^d = q_a^{(1),d}$. Now this solution can be imposed to the first underactuated sub-system using

$$u_1^{ext} = \Big(B_a^{(1)}\Big)^{-1}\Big(D_{aa}^{(1)} v_1^{ext} + D_{au}^{(1)} \ddot{q}_u^{(1)} + H_a^{(1)}\Big) \tag{3.28}$$

and

$$v_1^{ext} = \ddot{q}_a^{(1),d} + k_D\Big(\dot{q}_a^{(1),d} - \dot{q}_a^{(1)}\Big) + k_P\Big(q_a^{(1),d} - q_a^{(1)}\Big). \tag{3.29}$$

While this control is applied, the next underactuated sub-system must be kept balanced, hence the BEM $\mathcal{E}_2 = \{q_u^{(2),e} = \begin{bmatrix}\vartheta_2 & \vartheta_3\end{bmatrix}^T\}$ is explored by solving the equation for Γ_2.

u_2^{ext} and v_2^{ext} can be defined by repeating this process another time and then finding $\mathcal{E}_3 = \{q_a^3 = \vartheta_3\}$. Since the last system is fully actuated, the reference can be imposed using

$$u_3^{int} = \Big(B^{(3)}\Big)^{-1}\Big(D^{(3)} v_3^{int} + H^{(3)}\Big) \tag{3.30}$$

and

$$v_3^{int} = \ddot{q}_a^{(3),d} + k_D\Big(\dot{q}_a^{(3),d} - \dot{q}_a^{(3)}\Big) + k_P\Big(q_a^{(3),d} - q_a^{(3)}\Big). \tag{3.31}$$

The control laws obtained for each step are interconnected as follows. To make the last stage virtually actuated, recall the control comes from the previous cyclic stage of $\mathcal{S}_2$, leading to the feedback

$$u_2^{int} = \Big(B_a^{(2)}\Big)^{-1}\Big(D_{aa}^{(2)} v_2^{int} + D_{au}^{(2)} \ddot{q}_u^{(2)} + H_a^{(2)}\Big) \tag{3.32}$$

and

$$v_2^{int} = \Big(D_{aa}^{(2)}\Big)^{-1}\Big(B_a^{(2)} u_3^{int} - D_{au}^{(2)} v_3^{int} - H_a^{(2)}\Big), \tag{3.33}$$

where the first control u_2^{int} imposes the desired acceleration to the actuated coordinate $\ddot{q}_a^{(2)}$ inverting (3.15) for the second sub-system, then the second signal v_2^{int} brings the correct controls to the underactuated sub-system $\mathcal{S}_3$.

This procedure must be iterated because the controller for this stage comes from the previous sub-system $\mathcal{S}_1$ leading to the control signal

$$u_1^{int} = \Big(B_a^{(1)}\Big)^{-1}\Big(D_{aa}^{(1)} v_1^{int} + D_{au}^{(1)} \ddot{q}_u^{(1)} + H_a^{(1)}\Big) \tag{3.34}$$

and

$$v_1^{int} = \Big(D_{aa}^{(1)}\Big)^{-1}\Big(B_a^{(1)} u_2^{int} - D_{au}^{(1)} \begin{bmatrix} v_2^{int} \\ \ddot{q}_u^{(2)} \end{bmatrix} - H_a^{(1)}\Big). \tag{3.35}$$

By iterating one last time, we can obtain the final controller for the real actuated coordinate as

$$u_0^{int} = D_{aa} v_0^{int} + D_{au} \ddot{q}_u + H_a \tag{3.36}$$

and

$$v_0^{int} = \Big(D_{aa}\Big)^{-1}\Big(u_1^{int} - D_{au} \begin{bmatrix} v_1^{int} \\ \ddot{q}_u^{(1)} \end{bmatrix} - H_a\Big). \tag{3.37}$$

The general form of the i-th internal control is

$$u_i^{int} = \left(B_a^{(i)}\right)^{-1}\left(D_{aa}^{(i)} v_i^{int} + D_{au}^{(i)} \ddot{q}_u^{(i)} + H_a^{(i)}\right) \tag{3.38}$$

and

$$v_i^{int} = \left(D_{aa}^{(i)}\right)^{-1}\left(B_a^{(1)} u_{i+1}^{int} - D_{au}^{(i)} \begin{bmatrix} v_{i+1}^{int} \\ \ddot{q}_u^{(i+1)} \end{bmatrix} - H_a^{(i)}\right). \tag{3.39}$$

To prove that the (i)-th control u_i^{int} of previous sub-system imposes in closed loop the dynamics $\ddot{q}_a^{(i+1)} = v_{i+1}^{int}$, one can start by noticing this control signal performs a feedback linearization of the correspondent sub-system $\mathcal{S}^{(i)}$, hence all the terms involved get simplified, leading to $\ddot{q}_a^{(i)} = v_i^{int}$. After this, the proof proceeds by analysing the underactuated part of the subsystem $\mathcal{S}_a^{(i+1)}$:

$$\mathcal{S}_a^{(i+1)} : D_{aa}^{(i+1)} \ddot{q}_a^{(i+1)} + D_{au}^{(i+1)} \ddot{q}_u^{(i+1)} + H_a^{(i+1)} = B_a^{(i+1)} u_i^{int}. \tag{3.40}$$

Focusing on $B_a^{(i+1)} u_i^{int}$ and substituting the expression of u_i^{int} as in (3.38), we obtain

$$B_a^{(i+1)} u_i^{int} = B_a^{(i+1)}\left(B_a^{(i)}\right)^{-1}\left(D_{aa}^{(i)} v_i^{int} + D_{au}^{(i)} \ddot{q}_u^{(i)} + H_a^{(i)}\right) \tag{3.41}$$

where the term $D_{aa}^{(i)} v_i^{int}$ can be expanded using the expression of v_i^{int} in (3.39), so that the complete expression of (3.41) becomes

$$B_a^{(i+1)}\left(B_a^{(i)}\right)^{-1}\left(B_a^{(i)} u_{i+1}^{int} - D_{au}^{(i)} \begin{bmatrix} v_{i+1}^{int} \\ \ddot{q}_u^{(i+1)} \end{bmatrix} - H_a^{(i)} + D_{au}^{(i)} \ddot{q}_u^{(i)} + H_a^{(i)}\right) \tag{3.42}$$

or, recalling the equality $\ddot{q}_u^{(i)} = [\ddot{q}_a^{(i+1)}, \ddot{q}_u^{(i+1)}]^T$,

$$B_a^{(i+1)} u_i^{int} = B_a^{(i+1)} u_{i+1}^{int} + B_a^{(i+1)}\left(B_a^{(i)}\right)^{-1} D_{au}^{(i)} \begin{bmatrix} \ddot{q}_a^{(i+1)} - v_{i+1}^{int} \\ 0 \end{bmatrix}. \tag{3.43}$$

Substituting once more the expression of u_{i+1}^{int} as in (3.38) the equation reaches the form of

$$B_a^{(i+1)}\left(B_a^{(i)}\right)^{-1} D_{au}^{(i)} \begin{bmatrix} \ddot{q}_a^{(i+1)} - v_{i+1}^{int} \\ 0 \end{bmatrix} + D_{aa}^{(i+1)} v_{i+1}^{int} + D_{au}^{(i+1)} \ddot{q}_u^{(i+1)} + H_a^{(i+1)}. \tag{3.44}$$

After some manipulations and simplifications, the equation of $\mathcal{S}_a^{(i+1)}$ becomes

$$\left(D_{aa}^{(i+1)} - B_a^{(i+1)}\left(B_a^{(i)}\right)^{-1} D_{au}^{(i)}\right) \begin{bmatrix} \ddot{q}_a^{(i+1)} - v_{i+1}^{int} \\ 0 \end{bmatrix} = 0, \tag{3.45}$$

leading to the solution $\ddot{q}_a^{(i+1)} = v_{i+1}^{int}$ as desired.

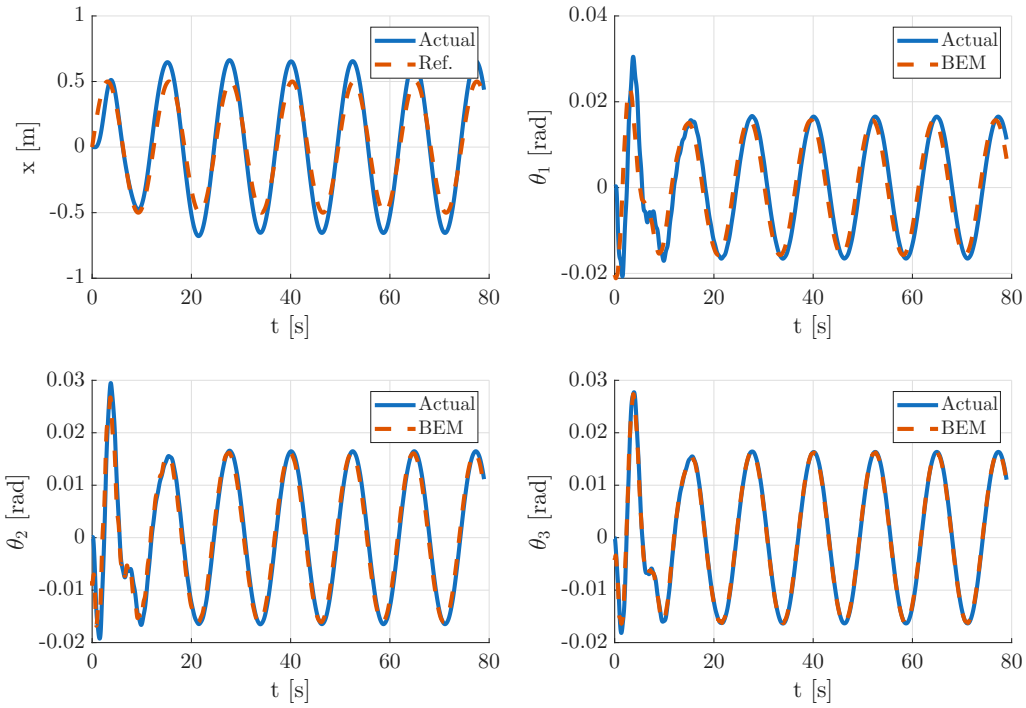

Figure 3.1: Joints and BEM under reference trajectory

3.3 Simulations

In this section we show simulation results using the CEIC method. The reference trajectory is $q_a^{(0),d} = 0.5\sin(0.5t)$. In these simulations, $q_u^{(i),e}$ is obtained not analytically, but by numerical optimization of Γ_{i+1} using `fmincon` in MATLAB, and assuming $\dot{q}_u^{(i),e} = \ddot{q}_u^{(i),e} = 0$. Figure 3.1 shows the resulting joint trajectories . As it's also seen from Figure 3.2, the last joint tracks the BEM perfectly, with the errors gradually increasing almost consistently by orders of magnitude for joints closer to the cart.

Finally, Figure 3.3 shows the Phase Portrait of each joint under the reference trajectory. The phase portrait settles into an elliptic trajectory after transient, showing stability of the system.

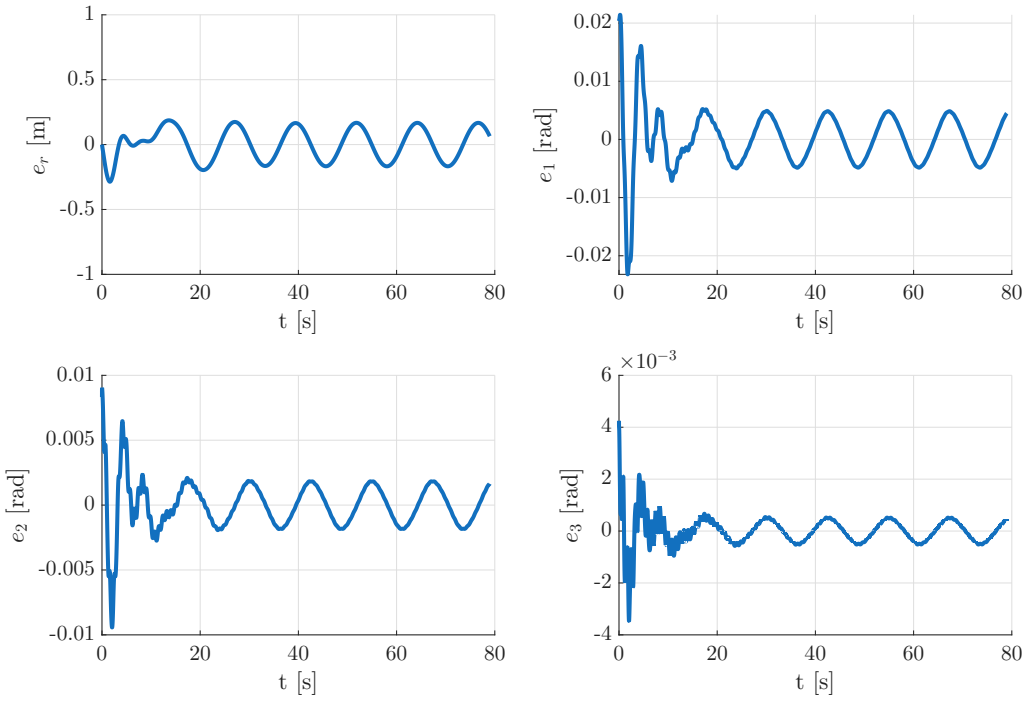

Figure 3.2: Errors w.r.t BEM under reference trajectory

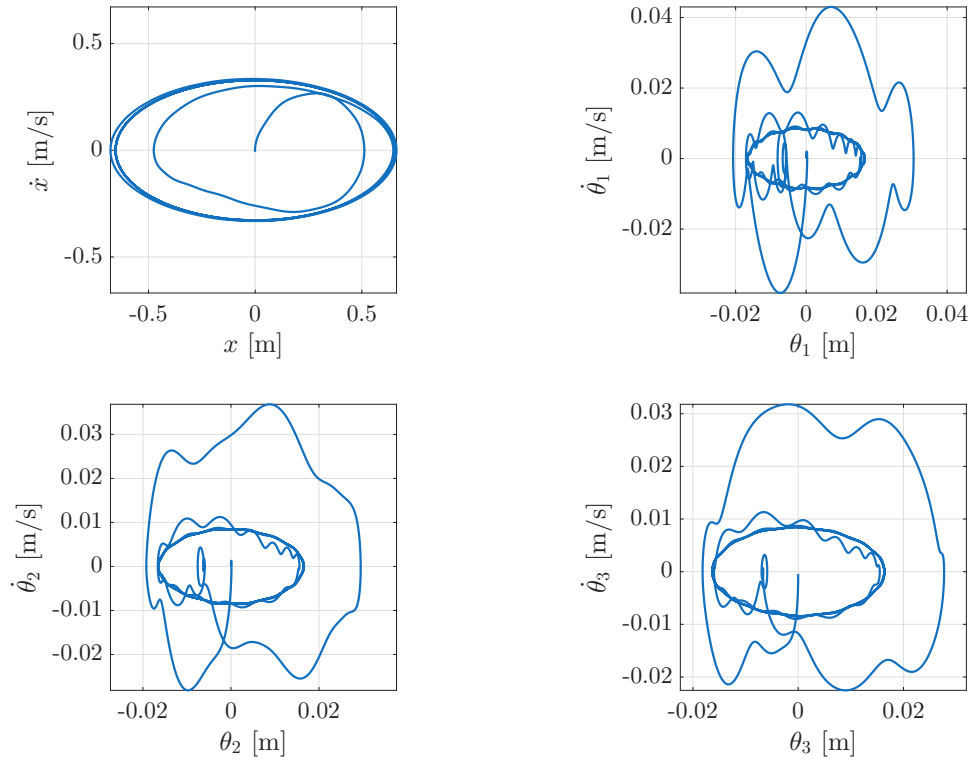

Figure 3.3: Phase Portrait

Conclusions

This project addressed the control of a triple inverted pendulum on a cart, which is a representative example of a highly underactuated nonlinear system. Due to the presence of three unactuated links and only one control input, there are significant challenges in terms of trajectory generation and stabilization.

The main objective of the project was to reproduce in simulation the results of of [3], which aims at generating and stabilizing a non-trivial periodic orbit of the system. In particular, we were successful in defining a cart trajectory that results in a stable periodic motion of continuous rotation for the third link. Furthermore, we were able to also implement a swing-up motion trajectory, to bring the robot from the downwards equilibrium to the upwards one, and an entry manoeuvrer which imparts the correct angular velocity to the third link to start from rest and initiate the period motion. We were also able to implement a defuse and swing-down manoeuvrer to stop the periodic motion and bring the robot back to the downwards equilibrium in a controlled manner, avoiding chaotic motion.

The main drawback of this approach is the difficulty in finding the right reference trajectory and, in particular, the susceptibility of the BVP solver to numerical conditioning. In fact, even small differences in the initial conditions of the solver, or in the duration of the trajectory, result in wildly different trajectories and control efforts, or in the impossibility of finding a solution at all. The problem can be at least automated by implementing a grid search approach for these parameters, as suggested by the authors. Still, even when a solution is found, it may be deemed unfeasible due to high control effort required. Finally, the LQR is valid only when the robot is already close to the nominal trajectory, which is ensured by the feedforward designed via BVP, therefore an accurate dynamic model of the robot is required for correct design.

In addition to the replication of the periodic orbit stabilization method, we also investigated the CEIC control framework proposed by [2]. This approach is specifically designed for highly underactuated systems, where classical EIC-based control cannot be directly applied. Indeed, standard EIC relies on the pseudoinverse of the coupling matrix $D_{ua} \in \mathbb{R}^{m \times n}$, which loses rank when $n < m$, so that the nonlinear terms in the unactuated dynamics cannot be fully cancelled and balance of the pendulum links is no longer guaranteed. The CEIC method addresses this limitation by recursively decomposing the

system into a cascade of subsystems that can be sequentially controlled through virtual actuation, each obtained by substituting the actuated dynamics into the unactuated one. For the triple pendulum on a cart, three nested subsystems are obtained, ending in a fully actuated scalar dynamics in ϑ_3. The control is constructed layer by layer: virtual inputs are designed top-down to drive each coordinate towards its instantaneous equilibrium, and then updated bottom-up to propagate the balance task back to the physical actuator. Simulation-wise, the main results presented in the reference paper, i.e. tracking of a sinusoidal trajectory for the cart, was replicated.

This approach has the main drawback of being analytically very complex, requiring computation of higher order derivatives of both the reference trajectory and the BEM of each joint, but simplifying assumptions can be made when implementing the controller. However, the approach also has the drawback of being extremely sensitive to PD gains, and in our tests has shown to not be robust to changes in dynamic parameters.

Overall, the two approaches tackle different control problems: BVP-LQR is concerned with tracking of pre-defined trajectories for the joints, while CEIC only regards balancing of the joints while tracking a trajectory for the cart alone.

Bibliography

[1] T. Glück, A. Eder, and A. Kugi. Swing-up control of a triple pendulum on a cart with experimental validation. *Automatica*, 49(3):801–808, 2013.

[2] F. Han and J. Yi. Cascaded nonlinear control design for highly underactuated balance robots. In *2024 American Control Conference (ACC)*, pages 581–586. IEEE, 2024.

[3] B. Jahn, L. Watermann, and J. Reger. On the design of stable periodic orbits of a triple pendulum on a cart with experimental validation. *Automatica*, 125:109403, 2021.